Effect of Viscoelasticity in the Film-Blowing Process

Michel Beaulne,[1] Evan Mitsoulis[2]

[1]*Department of Chemical Engineering, University of Ottawa, Ottawa, Ontario, Canada K1N 6N5*
[2]*School of Mining Engineering and Metallurgy, National Technical University of Athens, Zografou 157 80, Athens, Greece*

Received 17 November 2006; accepted 24 January 2007
DOI 10.1002/app.26325
Published online 3 May 2007 in Wiley InterScience (www.interscience.wiley.com).

ABSTRACT: Numerical simulations have been undertaken for the film-blowing process of viscoelastic fluids under different operating conditions. Viscoelasticity is described by an integral constitutive equation of the K-BKZ type with a spectrum of relaxation times, which can fit the experimental data well for the shear and extensional viscosities and the normal stresses measured in shear flow. Nonisothermal conditions are considered by applying the Morland–Lee hypothesis, which incorporates the appropriate shift factor and pseudotime into the constitutive equation. The momentum and energy equations are expressed in the machine direction only by using a quasi-one-dimensional approach introduced earlier by Pearson and Petrie. The resulting system of differential equations is solved using the finite element method and the Newton-Raphson iterative scheme. The method of solution was first checked against the Newtonian and Maxwell results for various film characteristics given earlier. The simulations are compared with available experimental data and previous simulations in terms of film shape, velocity, stresses, and temperature. The present results show that the existing modeling of force balances is inadequate for quantitative agreement with the experimental studies. © 2007 Wiley Periodicals, Inc. J Appl Polym Sci 105: 2098–2112, 2007

Key words: nonisothermal film blowing; K-BKZ constitutive equation; viscoelasticity; quasi-one-dimensional approach

INTRODUCTION

The film-blowing process is used industrially to manufacture plastic films that are biaxially oriented. Many attempts have been made to predict and model this complex but important process, which continues to mystify rheologists and polymer processing engineers worldwide. A constitutive equation, able to predict well the polymer melt in all forms of deformation, is required to model the process, together with the standard conservation equations of continuity, momentum, and energy. Pearson and Petrie[1,2] were the first to predict the forces within the blown film by the use of the thin-shell approximation, force balances, and the Newtonian constitutive equation. The use of the thin-shell approximation and force balances is standard in any attempt to model the film-blowing process and is also used in this work.

The process itself is portrayed in Figure 1, where a polymer melt is extruded through an annular die, and biaxial extension is effected by slight internal pressurization and axial drawing. Cooling air is supplied by air ring jets surrounding the mid- to upper-portion of the bubble. The height above the die at which solidification occurs, also known as the *freeze-line*, can be controlled by the cooling air. The deformation of the bubble, as well as changes in velocity and temperature, are negligible above the freezeline in most processes. The bubble dimensions are measured in terms of the *blow-up ratio*, the *draw ratio*, and the *thickness reduction*. The blow-up ratio (BUR), which is the ratio of the bubble radius at the freezeline to the inner die radius, is typically in the range of 1–4. The draw ratio (DR) is the ratio of the velocity at the freezeline to that of the average velocity at the die, and is typically in the range of 10–40. The thickness reduction (TR) is the ratio of the die annular spacing to the thickness at the freezeline, and is typically in the range of 20–200. The bubble is then flattened by a set of guide rolls and taken up by a set of nip rolls that form an airtight seal at the upper end of the bubble, thus forming a double-layered collapsed tube or sheet. Finally, the film is wound onto reels and sold as ''lay-flat'' tubing or trimmed at the edges and wound into two reels of flat film. While the film is being drawn and blown, it undergoes nonuniform biaxial deformation. The biaxial extension of the film is the primary attraction of the film-blowing process, which increases the strength of the film in two directions and allows for precise control over the mechanical, shrink, and optical properties of the final product.

There have been numerous previous studies on the film-blowing process. The first to model the process

Correspondence to: E. Mitsoulis (mitsouli@metal.ntua.gr).
Contract grant sponsors: Natural Sciences and Engineering Research Council (NSERC) of Canada, Ontario Centre for Materials Research (OCMR).

Journal of Applied Polymer Science, Vol. 105, 2098–2112 (2007)

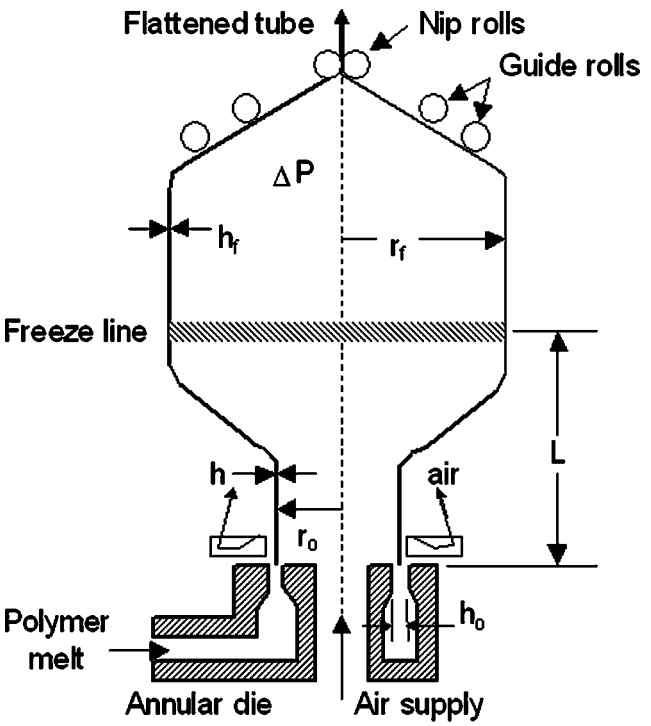

Figure 1 Sketch of the film-blowing process. A viscoelastic fluid is extruded through an annular die and is taken up at the nip rolls. Biaxial extension is effected by the drawing force at the nip rolls and by the blow-up pressure ΔP.

were Pearson and Petrie,[1,2] who derived a set of differential equations based on the thin-shell approximation, a force balance, and the deformation of a Newtonian fluid. Since the initial model proposed by Pearson and Petrie,[1,2] various rheological models have been incorporated in simulations, such as the power-law model,[3] a crystallization model,[4] the Maxwell model,[5–8] the Leonov model,[8] a viscoplastic-elastic model,[9] the PSM model,[10] and a nonisothermal viscosity model.[11] An investigation of the stresses of the film-blowing process with the differential equations from Pearson and Petrie[1,2] was reported by Kurtz,[12] who discovered an error in the work by Alaie and Papanastasiou.[10] Han and Park,[3] Kanai and White,[4] and Minoshima and White[13] have reported observations of flow instabilities in film-blowing experiments. Ghaneh–Fard et al.[14–17] conducted birefringence and instability film-blowing experiments with high-density and low-density polyethylenes. A complete set of experimental data was reported by Gupta[18] for the Styron 666 polystyrene (PS), and by Tas[19] for three different grades of low-density polyethylene (LDPE).

In this work, the film blowing of polymer melts is examined under isothermal and nonisothermal conditions. The constitutive equation used is the modified PSM integral constitutive equation with multiple relaxation times, proposed by Papanastasiou et al.[20] This model fits the data well for both shear and extensional viscosities, as well as normal stresses measured in shear. The effects of temperature are included into the constitutive equation by means of the Morland–Lee hypothesis,[21] which incorporates the Arrhenius shift-factor as well as the concept of ''pseudotime.'' This concept is based on the relative difference between the observer's time scale and the material's time scale. Both the momentum and energy equations are solved simultaneously, since they are coupled by the time-temperature shift factor by which the pseudotime is defined.

The purpose of this work is to compare the current numerical scheme, which utilizes the finite element method (FEM) and integral constitutive equations, with previous simulations that normally utilize the Runge–Kutta (R-K) method and differential constitutive equations. Further conclusions are drawn with respect to the Morland–Lee hypothesis[21] and the shifting of relaxation times.[22] Finally, simulations are undertaken for a real film-blowing experiment,[19] where the current mathematical modeling of the process, as well as previous ones, appear to be inadequate in terms of quantitative predictions for the film radius and film velocity.

MATHEMATICAL MODELLING

Governing equations for isothermal Newtonian film blowing

The analysis of the stresses and forces within the blown film follows the classic analysis by Pearson and Petrie,[1,2] where the film is regarded as a thin shell in tension. The equations are summarized below for completeness. For highly viscous fluids, viscous effects dominate the process so that inertia, gravity, and surface tension effects can be neglected. The assumption made that the bubble is axisymmetric allows the problem to be set up using a local coordinate system described by the unit vectors $\bar{s}$, $\bar{t}$, $\bar{n}$, respectively, in the machine, transverse, and normal directions from the inside of the sheet (Fig. 2).

Mass conservation demands that for incompressible materials

$$\rho 2\pi r h u_s = \rho Q = \text{constant} \tag{1}$$

where ρ is the density, Q is the volumetric flow rate, u_s is the machine-direction velocity component, h is the local film thickness, and r is the local bubble radius. Taking the derivative of eq. (1) with respect to the arc length normal $\bar{s}$, as shown in Figure 2, results in

$$\frac{1}{u_s}\frac{du_s}{ds} = -\frac{1}{h}\frac{dh}{ds} - \frac{1}{r}\frac{dr}{ds} \tag{2}$$

The left-hand side of eq. (2) is the rate of machine-direction stretching along the film, and the two terms

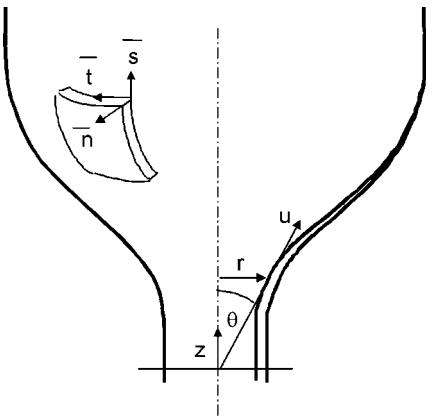

Figure 2 Film curvature definition in terms of the moving coordinate system with unit vectors $\bar{s}$, $\bar{t}$, and $\bar{n}$ in the machine direction, transverse (hoop) direction, and normal direction, respectively. Note the reference point is located on the inside surface of the bubble.

on the right-hand side are, respectively, the negatives of the stretch rates in the thickness direction, $\bar{n}$, and the transverse direction, $\bar{t}$. Normal force equilibrium occurs when

$$\frac{\Delta P}{h} = \frac{\tau_{ss}}{R_s} + \frac{\tau_{tt}}{R_t} \tag{3}$$

where τ_{ss} and τ_{tt} are the cross section averaged machine-direction and transverse stresses, R_s and R_t are the principal curvatures in the two directions $\bar{s}$ and $\bar{t}$, and ΔP is the internal pressure measured relative to the external (atmospheric) one. By means of simple differential geometry principles, it can be shown that

$$R_s = -\frac{\left[1 + \left(\frac{dr}{dz}\right)^2\right]^{3/2}}{\frac{d^2r}{dz^2}} \tag{4}$$

$$R_t = r\left[1 + \left(\frac{dr}{dz}\right)^2\right]^{1/2} \tag{5}$$

A force balance in the direction of the axis of symmetry, z, results in,

$$F = 2\pi r h \tau_{ss} \cos\theta + \pi \Delta P\left(r_L^2 - r^2\right) \tag{6}$$

where F is the applied tension at distance $z = L$, and r_L is the final bubble radius at distance $z = L$. Equations (1) and (6) are made dimensionless by means of the following dimensionless variables

$$r^* = \frac{r}{r_o}, \quad z^* = \frac{z}{r_o}, \quad u^* = \frac{u}{u_o}, \quad \tau^* = \frac{\tau}{\eta_o u_o / r_o} \tag{7}$$

where r_o is the inner radius of the annulus, u_o is the average velocity of the fluid within the die, and η_o is the zero-shear-rate viscosity of the fluid. The resulting dimensionless equations, through the use of the dimensionless variables in eq. (7) and by combining eqs. (1)–(6) with asterisks suppressed hereafter, are

$$\left(A + r^2 B\right)\frac{d^2r}{dz^2} + 2rB\left[1 + \left(\frac{dr}{dz}\right)^2\right] - \frac{\tau_{tt}}{ur}\left[1 + \left(\frac{dr}{dz}\right)^2\right]^{1/2} = 0 \tag{8}$$

$$\tau_{ss} - u\left(A + r^2 B\right)\left[1 + \left(\frac{dr}{dz}\right)^2\right]^{1/2} = 0 \tag{9}$$

with the two dimensionless constants defined as

$$A = \frac{Fr_o}{\eta_o Q} - B\left(\frac{r_L}{r_o}\right)^2 \tag{10}$$

$$B = \frac{\pi \Delta P r_o^3}{\eta_o Q} \tag{11}$$

The Newtonian stresses can be easily deduced from Newtonian deformation theory and are given as

$$\tau_{ss} = 2u \cos\theta\left[\frac{1}{r}\frac{dr}{dz}\right] \tag{12}$$

$$\tau_{tt} = 2u \cos\theta\left[\frac{1}{r}\frac{dr}{dz} - \frac{1}{h}\frac{dh}{dz}\right] \tag{13}$$

Eqs. (8) through (13), when combined, give the well-known governing equations for film blowing

$$2r^2\left(A + r^2 B\right)\frac{d^2r}{dz^2} = 6\frac{dr}{dz} + r\left[1 + \left(\frac{dr}{dz}\right)^2\right]\left(A - 3r^2 B\right) \tag{14}$$

$$\frac{dh}{dz} = -h\left[\frac{\frac{dr}{dz}}{2r} + \frac{\left[1 + \left(\frac{dr}{dz}\right)^2\right]\left(A + r^2 B\right)}{4}\right] \tag{15}$$

These equations are solved here by the finite element method to obtain initial estimates for the viscoelastic case, and also to validate the viscoelastic constitutive equation when reduced to its Newtonian limit.

Governing equations for nonisothermal viscoelastic film blowing

To proceed with the analysis of a viscoelastic fluid, the stresses τ_{ss} and τ_{tt} in eqs. (8) and (9) must be expressed in terms of the velocity by means of a constitutive equation. The one chosen here is the PSM integral constitutive equation with multiple relaxation times, proposed by Papanastasiou et al.[20] and further

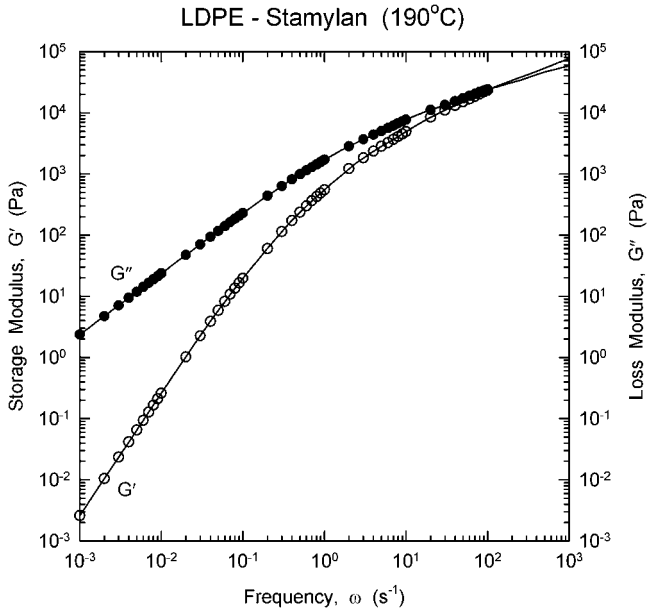

Figure 3 Predictions (solid lines) by the PSM model of the experimental data (symbols) for the storage and loss modulus for the L8 Stamylan low-density polyethylene (LDPE) used by Tas.[19] Material parameters are given in Table I.

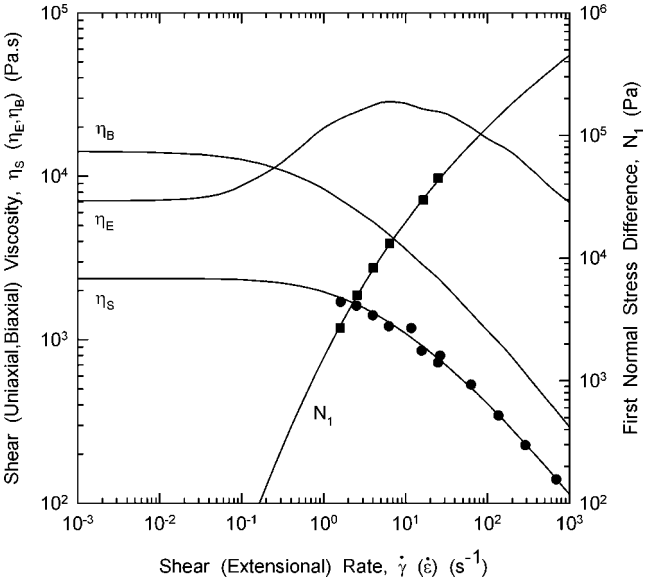

Figure 4 Predictions (solid lines) by the PSM model of the experimental data (symbols) for the steady shear, uniaxial, and biaxial viscosities as well as the first normal stress difference for the L8 Stamylan low-density polyethylene (LDPE) used by Tas.[19] Material parameters are given in Table I.

modified by Luo and Tanner.[23] This is written as

$$\tau = \frac{1}{1-\theta}\int_{-\infty}^{t}\sum_{k=1}^{N}\frac{a_k}{\lambda_k}\exp\left(-\frac{t-t'}{\lambda_k}\right) \times \frac{\alpha_k}{(\alpha_k-3)+\beta_k\mathbf{I}_{C^{-1}}+(1-\beta_k)\mathbf{I}_C} \times \left(\mathbf{C}_t^{-1}(t')+\theta\mathbf{C}_t(t')\right)dt' \quad (16)$$

where N is the number of relaxation modes, λ_k and a_k are the relaxation times and relaxation moduli at a reference temperature T_o, α_k, and β_k are material constants, and $\mathbf{I}_C$,$\mathbf{I}_{C^{-1}}$ are the first invariants of the Cauchy–Green tensor $\mathbf{C}_t$ and its inverse $\mathbf{C}_t^{-1}$, the Finger strain tensor. The material constant θ is given by

$$\frac{N_2}{N_1} = \frac{\theta}{1-\theta} \quad (17)$$

where N_1 and N_2 are the first and second normal stress differences, respectively. Note that θ is not zero for polymer melts exhibiting a second normal stress difference, such as low-density polyethylene melts. Its usual range is between -0.1 and -0.2.[21] In the present work, a value of $\theta = -1/9$ has been used.

The above eq. (16) reduces to the well-known upper-convected Maxwell (UCM) model in the case of a single relaxation time λ and its corresponding relaxation modulus a, a large value of α (say $\alpha = 10{,}000$), a value for β between 0 and 1, and $\theta = 0$. The UCM model is routinely used for validation purposes of a viscoelastic scheme, and as such it will be dealt with here as well.

The material under study is the L8 Stamylan low-density polyethylene (LDPE) used by Tas.[19] Nonlinear regression was performed for this material using the above constitutive equation, eq. (16), to find the spectrum of relaxation times λ_k, and coefficients, a_k, as well as the material parameters α (shear-thinning parameter) and β (extensional parameter). Figure 3 displays the dynamic moduli G' and $G,''$ while Figure 4 displays the shear viscosity, η_S, uniaxial extensional viscosity, η_E, biaxial extensional viscosity, η_B, and the first normal stress difference, N_1, together with the model predictions. The values of the parameters in eq. (16) for LDPE are given in Table I.

The viscoelasticity of the material under flowing conditions can be represented by the dimensionless variable known as the Weissenberg number, *Ws*, given as

TABLE I
Material Parameters Used in eq. (16) for the L8 Stamylan Low-Density Polyethylene (LDPE) at 190°C Used in the Experiments by Tas[19] (α = 12.82, β = 0.058, θ = −0.111, η_o = 2365.0 Pa s)

k	λ_k (s)	a_k (Pa)
1	4.28×10^{-5}	2.17×10^{5}
2	2.07×10^{-4}	9.18×10^{4}
3	1.34×10^{-3}	5.75×10^{4}
4	9.02×10^{-3}	2.43×10^{4}
5	5.69×10^{-2}	8.91×10^{3}
6	3.44×10^{-1}	2.34×10^{3}
7	1.82	321
8	9.94	12.4

$$Ws = \frac{u_o}{r_o}\frac{\sum a_k \lambda_k^2}{\sum a_k \lambda_k} = \frac{u_o}{r_o}\bar{\lambda} \tag{18}$$

where $\bar{\lambda}$ is the average relaxation time. For the isothermal case, the transit times along the film are given, in terms of the velocity and distance traveled, by

$$t - t' = \int_{s'}^{s} \frac{ds''}{u(s'')} \tag{19}$$

with

$$\frac{ds''}{dz''} = \frac{1}{\cos\theta} = \left[1 + \left(\frac{dr}{dz}\right)^2\right]^{1/2} \tag{20}$$

where double prime ($''$) denotes a position between s and s'. The traveling times are used within the modified PSM equation, where a time $t' < 0$ indicates that the history of the particle is within the annulus (prehistory), and a time $0 < t' < t$ indicates that history of the particle is within the blown film (history). The stress of the fluid particle, $\tau(t')$, which at present time t, occupies a position s, is a function of the Finger strain tensor $\mathbf{C}_t^{-1}$, to which the particle had been exposed in moving from far away to its present position s, along the streamline ∞ ($<s' <s''$). The Finger strain tensor is defined differently, based on whether the history of the particle is within the annulus or within the blown film. The two definitions for the Finger strain tensor are:

i. The Finger strain tensor, $\mathbf{C}_t^{-1}$, between the present location s of velocity $u(s)$ and past locations in the same extensional (biaxial) field of velocity $u(s')$:

$$\mathbf{C}_t^{-1}(t') = \begin{bmatrix} \left[\frac{u(s)}{u(s')}\right]^2 & 0 & 0 \\ 0 & \left[\frac{u(s')r(s')}{u(s)r(s)}\right]^2 & 0 \\ 0 & 0 & \left[\frac{r(s)}{r(s')}\right]^2 \end{bmatrix} \tag{21}$$

ii. The Finger strain tensor, $\mathbf{C}_t^{-1}$, between the present location s of velocity $u(s)$ and past locations in the extensional (planar) prehistory field of velocity $u(s')$:

$$\mathbf{C}_t^{-1}(t') = \begin{bmatrix} \left[\frac{u(s)}{u(s')}\right]^2 & 0 & 0 \\ 0 & \left[\frac{u(s')(1)}{u(s)r(s)}\right]^2 & 0 \\ 0 & 0 & \left[\frac{r(s)}{(1)}\right]^2 \end{bmatrix} \tag{22}$$

since $r(s') = 1$ within the die, in dimensionless form.

In the nonisothermal case, it is necessary to derive a nonisothermal constitutive equation from the isothermal one. This is done by applying the time-temperature shifting concept as explained by Luo and Tanner.[22] This concept is based on the relative difference between the observer's time scale and the material's time scale. Using ξ for the time measured by the material's own internal clock, the following relation holds between ξ and the observer's time t,

$$d\xi = \frac{dt}{a_T(T)} \tag{23}$$

where the denominator is the time-shifting factor.[21] The above relationship expresses the Morland–Lee hypothesis[21] in a differential form and can be used to obtain the following integral relation between the particle's elapsed time and the observing period.

$$\xi = \int_0^t a_T^{-1}(T(t'))dt' \tag{24}$$

Thus as a fluid particle is tracked along a streamline segment Δs_i, the particle's time corresponding to the residence time $\Delta t'$ is given by

$$\Delta\xi' = \frac{\Delta s_i}{u_i a_T(T_i)} \tag{25}$$

In Figure 5 the path of the particle is sketched, and the relevant times and lengths are presented. The above eq. (23) can be used to obtain the nonisothermal form of the modified PSM equation by replacing the observer's time t in eq. (16) with the particle's time ξ given by eq. (23). The resulting version of the constitutive equation becomes

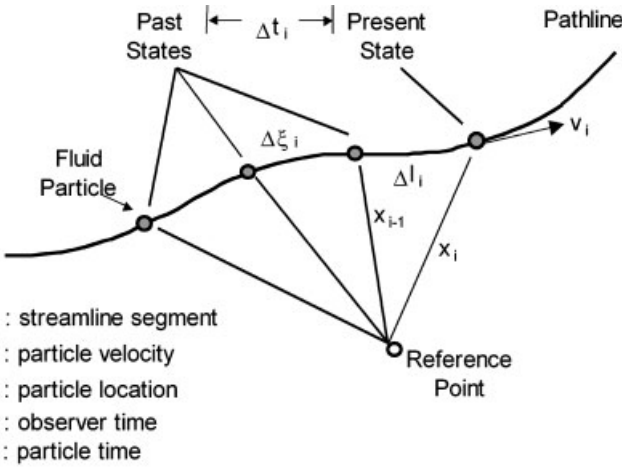

Figure 5 In steady-state flows of viscoelastic liquids, the present stress state of a fluid particle is a function of the particle's stress history (past states). For the nonisothermal case, the material's internal clock is not the same as the observer's clock according to the Morland–Lee hypothesis.[21]

$$\tau = \frac{1}{1-\theta}\int_{-\infty}^{\xi(t)} \sum_{k=1}^{N} \frac{a_k}{\lambda_k} \exp\left(-\frac{\xi-\xi'}{\lambda_k}\right) \times \frac{\alpha_k}{(\alpha_k-3)+\beta_k \mathbf{I}_{C^{-1}}+(1-\beta_k)\mathbf{I}_C} \times \left(\mathbf{C}^{-1}_{t(\xi)}(t'(\xi'))+\theta \mathbf{C}_{t(\xi)}(t'(\xi'))\right) d\xi' \quad (26)$$

The time-temperature shifting factor a_T is obtained from the Arrhenius equation and is given as

$$a_T = \exp\left[\frac{E}{R}\left(\frac{1}{T}-\frac{1}{T_{\text{ref}}}\right)\right] \quad (27)$$

where E is the activation energy, R is the ideal gas constant, and T_{ref} is the reference temperature for the material.

Another method can be applied to derive the nonisothermal constitutive equation from the isothermal one. This method is based on the time-temperature superposition principle and consists of shifting the relaxation times from the temperature history within the material's time scale.[22] The equation used to shift the relaxation times in the material's history is given as

$$\lambda(T'(z')) = \lambda(T_{\text{ref}})a_T(T'(z')) \quad (28)$$

Both methods are used to compare the relative predictive capabilities.

By assuming a uniform temperature over the cross section of the film and negligible axial heat conduction and viscous dissipation, the dimensionless energy equation for temperature simplifies to

$$\frac{dT}{dz} = -r\left[\gamma_1(T-T_a)+\gamma_2(T^4-T_a^4)\right] \quad (29)$$

where

$$\gamma_1 = \frac{2\pi r_o^2 H}{\rho c_P Q_o \cos\theta} \quad (30)$$

and

$$\gamma_2 = \frac{2\pi r_o^2 \varepsilon K T_o^3}{\rho c_P Q_o \cos\theta} \quad (31)$$

are dimensionless numbers with T_a, the dimensionless air temperature; c_P, the specific heat capacity; H, the heat transfer coefficient; ε, the emissivity; K, the Boltzmann radiation constant; and Q_o, the volumetric flow rate in the annular die. The density, ρ, and the specific heat capacity, c_P, change along the blown film distance, since these are functions of temperature. For the heat capacity of the polymer, the following expression, which was suggested by Haw,[24] was used

$$c_P(T) = c_P^o\left(\frac{k_1+k_2T}{k_1+k_2T_o}\right) \quad (32)$$

where c_p^o is the heat capacity at the reference temperature T_o, and k_1 and k_2 are empirical constants. The density ρ is given by

$$\rho = \frac{\rho_o}{1+c_\rho(T-T_o)} \quad (33)$$

where ρ_o is the density at temperature T_o, and c_ρ is a constant of expansion. The parameters used in this study for the nonisothermal simulations of the L8 Stamylan LDPE are given in Table II.

Special mention needs to be made for the heat transfer coefficient H, which is difficult to determine and there might be significant local variations, which may affect the rheology and the final predictions, as recent works[25,26] have made clear.

The prehistory kinematics needed in eq. (26) is inserted with the extensional prehistory given by the kinematics

$$u = \exp^{cz} \quad (34)$$

which originates from the Newtonian solution for planar elongation within an annular die (same solution as that for uniaxial elongation within a tube). This method is similar to the one used by Chen and Papanastasiou,[27] who employed uniaxial prehistory kinematics for their study of the fiber-spinning process. The parameter c is one of the unknowns to be determined simultaneously with the solution by requiring continuous stresses at the die exit.

TABLE II
Material Parameters Used in the Nonisothermal Simulations for the L8 Stamylan LDPE at 190°C Given by Tas[19]

Property (units)	Value
Density, ρ (g cm^{-3})	0.92
Activation energy, E_o (J mol^{-1})	57,500
Reference temperature, T_{ref} (°C, K)	190 (463)
Specific heat, $C_{P,o}$ (erg g^{-1} K^{-1})	2.302×10^7
Zero-shear-rate viscosity, η_o (Pas)	2365.0
Ideal gas constant, R (J mol^{-1} K^{-1})	8.314
Emissivity, ε	0.65
Stefan-Boltzmann constant, K (erg s^{-1} cm^{-2} K^4)	5.67×10^{-5}
Empirical constants, k_1 and k_2 (K^{-1}) in eq. (32)	1.454 and 0.000271
Coefficient of expansion, c_ρ in eq. (33)	0.00069
Heat transfer coefficient, H (erg cm^{-2} K^{-1})	40,000

Boundary conditions and specification of the freezeline position

The governing equations presented earlier, which describe the film-blowing process, are subjected to the following boundary conditions:

$$\text{at} \quad z = 0, \quad \begin{cases} r = r_o \\ u = u_o \\ T = T_o \end{cases} \qquad \text{at} \quad z = \frac{L}{r_o}, \quad \left\{ \frac{dr}{dz} = 0 \right. \tag{35}$$

It should be noted that the freezeline position is fixed *a priori*, consistent with previous studies.[2,7,8,10] When simulating experimental data, the freezeline position is chosen by inspecting the bubble radius and film velocity, and choosing a position where these variables become constant, i.e., the freezeline. Other nonisothermal simulations[11] have made predictions past the freezeline by choosing a suitable solidification temperature, where once the solidification temperature is reached, the viscosity is made infinite ($+\infty$). This causes the variables (bubble radius, velocity, temperature) to become constant. This method was not chosen here since it adds another adjustable parameter (the freezing temperature, T_f) to the numerical scheme. It is more appropriate to choose the freezeline position *a priori*, consistent with experimental data, rather than introducing another unknown variable (the freezeline position, L) along with another adjustable parameter (T_f).

The governing equations presented earlier describe the film-blowing process in the liquid (melt) region. Near the freezeline, the simulated bubble radius becomes constant because of the second imposed boundary condition (at $z = L/r_0$, $dr/dz = 0$), thus appearing to solidify as in the experiments. However, the velocity and temperature do not become constant near the freezeline, since imposing a similar boundary condition at the freezeline (as in the case for the radius) would overspecify the system of equations. Again, the governing equations presented earlier for the film-blowing process, are only valid in the liquid (melt) region.

METHOD OF SOLUTION

The unknown surface velocity u, the film profile r, and the temperature T, along the film, are approximated with quadratic finite element shape functions, ϕ^i:

$$u(z) = \sum_{i=1}^{3} u_i \phi^i(z), \quad i = 1, 2, \ldots, \text{NN} \tag{36}$$

$$r(z) = \sum_{i=1}^{3} r_i \phi^i(z), \quad i = 1, 2, \ldots, \text{NN} \tag{37}$$

$$T(z) = \sum_{i=1}^{3} T_i \phi^i(z), \quad i = 1, 2, \ldots, \text{NN} \tag{38}$$

where NN is the number of nodes. The differential equations pertaining to each variable [eqs. (8), (9), and (29)] are then weighted with the same shape functions as those used for each variable, and the resulting Galerkin weighted residuals with the appropriate boundary conditions are

$$R_r^1 = 0, \tag{39}$$

$$R_r^i = \int_0^1 \left\{ -\frac{dr}{dz}\frac{d\phi^i}{dz} + \left[\frac{1}{(A + r^2 B)} \left(2rB \left[1 + \left(\frac{dr}{dz} \right)^2 \right] - \frac{\tau_{tt}}{ru} \left[1 + \left(\frac{dr}{dz} \right)^2 \right]^{1/2} \right) \right] \phi^i \right\} dz = 0, \quad i = 2, \ldots, \text{NN}, \tag{40}$$

$$R_u^1 = 0, \tag{41}$$

$$R_u^i = \int_0^1 \left\{ \tau_{ss} - (A + r^2 B) \left[1 + \left(\frac{dr}{dz} \right)^2 \right]^{1/2} \right\} dz = 0, \quad i = 2, \ldots, \text{NN}, \tag{42}$$

$$R_T^1 = 0, \tag{43}$$

$$R_T^i = [T\phi^i]_{z=0}^{z=1} - \int_0^1 \left\{ T\frac{d\phi^i}{dz} - r[\gamma_1(T - T_a) + \gamma_2(T^4 - T_a^4)]\phi^i \right\} dz = 0, \quad i = 2, \ldots, \text{NN}, \tag{44}$$

All boundary residuals at the inlet are set to zero to impose the inlet radius, velocity and temperature. The stresses in the residual equations are replaced by the stresses defined by the modified PSM constitutive equation. The upstream memory resulting from the integral constitutive equation is computed via a 15-point Gauss–Laguerre quadrature suited for exponentially fading functions, as done in previous simulations for integral models,[23] while the Galerkin residuals are computed with Gauss–Legendre quadrature. The residuals, which are required to vanish, result in a system of 3(NN) nonlinear equations with the variables, $\mathbf{q} = \{r_1, r_2, \ldots, r_{\text{NN}}, u_1, u_2, \ldots, u_{\text{NN}}, T_1, T_2, \ldots, T_{\text{NN}}\}^{\mathbf{T}}$, as the unknowns. The equations are solved by the Newton–Raphson iterative scheme, i.e.,

$$[\mathbf{J}]\{\mathbf{q}^{(n+1)} - \mathbf{q}^{(n)}\} = -\{\mathbf{R}\{\mathbf{q}^{(n)})\} \tag{45}$$

where $\mathbf{R}$ is the vector of the Galerkin weighted residuals and $[\mathbf{J}]$ is the Jacobian matrix of the deriva-

TABLE III
Convergence Process for the Film-Blowing Program F-BLOW[27] for the Flow of the L8 Stamylan LDPE[19]

No. of elements	No. of nodes	No. of primary variables	No. of iterations	CPU (s/Iter)	Total CPU time (s)
46	93	3	6	48.2	291 (403)

CPU time is given for calculations on a workstation (IBM-RISC 6000/590). Numbers in parenthesis in the last column correspond to wall-clock time in seconds.

tives of the residuals with respect to the variable nodal values $\{\mathbf{q}^{(n)}\}$ for the nth iteration. The tensor notation for the Jacobian derivative is

$$J_{ij} = \frac{\partial R_i}{\partial u_j} \tag{46}$$

which is calculated numerically according to the definition of the derivative.

The method used for viscoelastic computations follows that of Barakos and Mitsoulis.[28] To that effect a finite-element program (F-BLOW) was written for simulations of the film-blowing process.[29] The Newtonian solution is first obtained with the viscoelastic equations at the limit of a small flow rate. The flow rate is then gradually increased to the required flow rate (thus increasing the level of viscoelasticity) using continuation of the primary variables. A converged solution was considered to have been reached for the nonlinear set of equations when the root-mean-square-of-the-error was below 10^{-4}. The iterative process is summarized in Table III. More details about the numerical aspects can be found in a thesis.[29]

RESULTS AND DISCUSSION

Newtonian case

To establish confidence in the numerical scheme implemented in this study, the solution of the Newtonian problem [eqs. (14) and (15)] was first solved with a fourth-order Runge–Kutta (R-K) procedure. At a very small Weissenberg number ($W_s = 0.001$), the viscoelastic case reduces to the Newtonian one. Therefore, the viscoelastic case is solved at a very small Weissenberg number with the FEM, which can then be evaluated against the Newtonian solution solved by R-K. The dimensionless force was chosen at $f = 2.9$, dimensionless pressure at $B = 0.2$, with a dimensionless length at $L/r_o = 5.0$, where the Newtonian solution under these conditions is well-documented.[2,8] Figure 6 shows the results of solving the viscoelastic solution at the limit of very small relaxation time approaching Newtonian behavior against the Newtonian solution at identical conditions. The viscoelastic solution gave identical radial and velocity profiles to that of the Newtonian solution, which verifies that our numerical scheme is valid at small Weissenberg numbers.

It was also found during the testing of the Newtonian solution against the viscoelastic case that an error is present in the study of Alaie and Papanastasiou.[10] In validating their numerical scheme against the Newtonian solution, they used a dimensionless force of $f = 2.3$, dimensionless pressure of $B = 0.2$, and a dimensionless length of $L/r_o = 7.0$. Under these conditions, the final dimensionless radius for the Newtonian solution is $r_L/r_o = 3.015$ and the final dimensionless velocity is $u_L/u_o = 6.593$. Alaie and Papanastasiou[10] report that their viscoelastic solution at $W_s = 0.001$ (Fig. 8 in Ref. [10]), which gave a final dimensionless radius of $r_L/r_o = 3.12$, and a final dimensionless velocity of $u_L/u_o = 11.8$, matched the Newtonian solution. This is a false claim and their numerical scheme validation is incorrect. Hence, their results for the viscoelastic case are indeed questionable. It should also be pointed out that their numerical scheme was not tested against any upper-convected Maxwell (UCM) model cases.

Maxwell case

To proceed with this analysis, the numerical scheme used in this study must also be valid at higher Weissenberg numbers. The upper-convected Maxwell

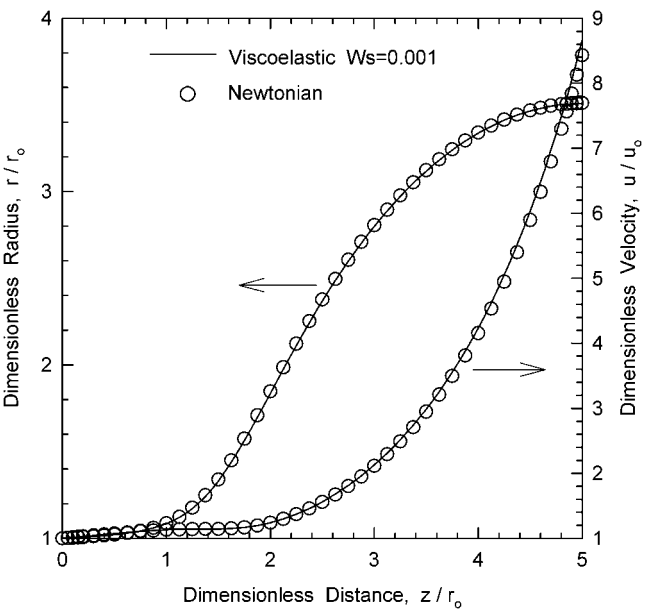

Figure 6 Predictions of the viscoelastic simulation (solid line) in the limiting case of low Weissenberg number ($Ws = 0.001$) compared with the Newtonian solution (open symbols). The dimensionless force is $f = 2.9$, the dimensionless pressure is $B = 0.2$, and the dimensionless length $L/r_o = 5.0$.

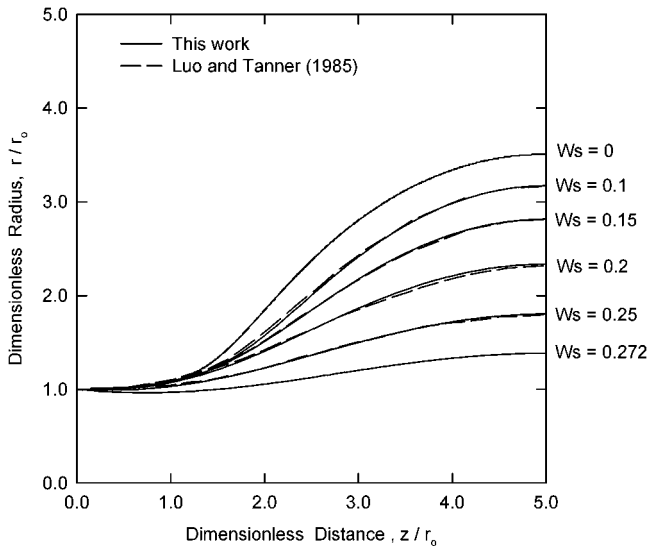

Figure 7 Predictions of the viscoelastic simulation (solid line) for the upper-convected Maxwell (UCM) limiting case compared with the UCM simulations by Luo and Tanner[8] (dashed line).

(UCM) model case is therefore analyzed at identical conditions to those of Luo and Tanner,[8] who performed a series of simulations of varying Weissenberg numbers at a dimensionless force of $f = 2.9$, dimensionless pressure of $B = 0.2$, and a length of $L/r_o = 5.0$ (identical to the Newtonian case). Figure 7 shows the results of this study for the UCM model against those of Luo and Tanner[8] at different Weissenberg numbers ($Ws = 0.1, 0.15, 0.2, 0.25$). The simulation results gave identical radial profiles reported by Luo and Tanner[8] at every Weissenberg number. This comparison verifies that our numerical scheme is valid for viscoelastic cases. Also shown in Figure 7 is the effect of increasing the Weissenberg number on the final radius, r_L, at $z = L$. As the Weissenberg number increases, the more solid (plastic) the material becomes and hence resists deformation, explaining the reduced bubble radius. Also shown is the simulation result for the Maxwell model at a higher Weissenberg number ($Ws = 0.272$) than previously reported by Luo and Tanner,[8] which was the limit for this study. The limiting case for the Maxwell model at even higher Weissenberg numbers would result in a completely flat radial and velocity profile (drawing of a solid tube).

It is interesting to note that two very dissimilar approaches to solving the film-blowing governing equations with the UCM model gave identical results. Luo and Tanner[8] used a fourth-order Runge-Kutta (R-K) procedure with the UCM differential constitutive equation to solve the film-blowing problem, where prehistory effects were handled by the convected derivative. This study used the finite element method (FEM) with the integral equivalent of the UCM model, where prehistory effects were handled with extensional kinematics, and the integral constitutive equation was solved with a 15-point Gauss–Laguerre quadrature.

Shear versus extensional prehistory

Before continuing with the analysis and simulation of reported film-blowing experiments, the difference between extensional prehistory and shear prehistory (the latter described in Ref. 10) will be analyzed. The study performed by Alaie and Papanastasiou[10] used a method very similar to the one used here, i.e., implementation of the PSM integral constitutive equation with the same film-blowing governing equations. The major difference is that this study uses an extensional prehistory described by eq. (34), while Alaie and Papanastasiou[10] used a shear prehistory. Initially, this study was also carried out with a shear prehistory. However, after numerous simulations with the Newtonian and upper-convected Maxwell (UCM) models, it was discovered that shear prehistory gave spurious stresses and sometimes incorrect radius and velocity profiles. Using a shear prehistory within the die with a sudden change to extensional history outside of the die, results in a singularity point in the quasi-one-dimensional analysis used in this study. This causes numerical instabilities in the stress calculations. To visualize this, the results of the UCM model at the same operating conditions as above, at a Weissenberg number of $Ws = 0.25$, are given for the

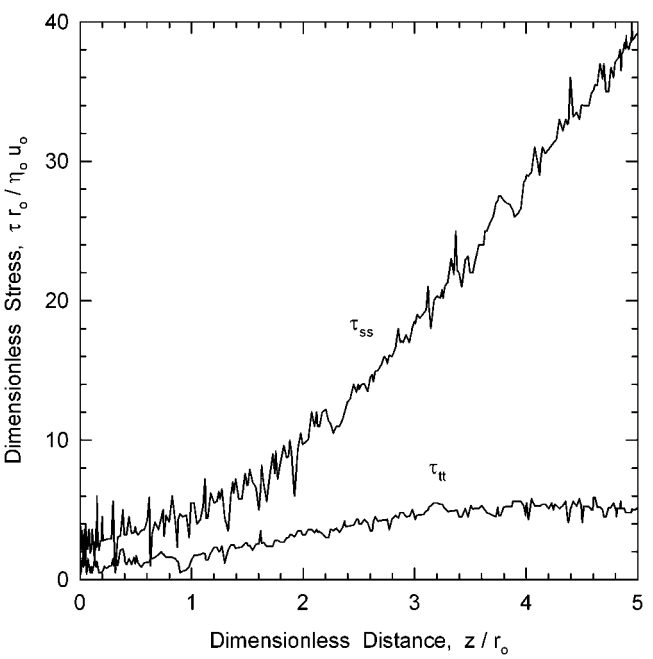

Figure 8 Predictions of the machine and hoop stresses of the viscoelastic simulation for the upper-convected Maxwell (UCM) limiting case at $Ws = 0.25$ using a shear prehistory.

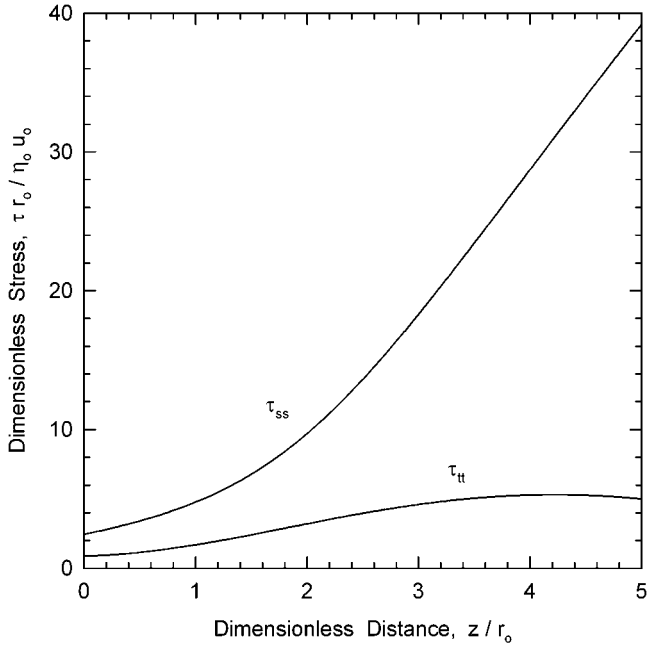

Figure 9 Predictions of the machine and hoop stresses of the viscoelastic simulation for the upper-convected Maxwell (UCM) limiting case at $Ws = 0.25$ using an extensional prehistory.

two cases, i.e., with shear prehistory and extensional prehistory. Figures 8 and 9 show the dimensionless stresses, τ_{ss}^* (machine-direction stress) and τ_{tt}^* (hoop-direction stress), for the shear prehistory and extensional prehistory, respectively. It can be seen in Figure 8 that a shear prehistory at higher Weissenberg numbers causes numerous oscillations in the calculation of the stresses, τ_{ss}^* and τ_{tt}^*. Also, it can be seen in Figure 9 that, at the same conditions, extensional prehistory results in a smooth stress profile. The smooth profile is also due to the condition, with extensional prehistory, that the stress be continuous inside and outside of the die. It is also interesting to note that the shear prehistory and extensional prehistory, although different in nature, give relatively the same magnitude of values for the stresses. This was also observed by Chen and Papanastasiou[27] in studying the two prehistory formulations for fiber spinning. The oscillatory behavior caused by the shear prehistory is simply a numerical issue for the current numerical scheme. Physically, the deformation within the die is mostly due to shear, and a shear prehistory experienced by the material would dominate.

TABLE IV
Material Parameters Used in the Nonisothermal Simulations of the Maxwell Test Cases for the Morland–Lee Hypothesis vs. the Shifting of Relaxation Times

Property (units)	Value
Density, ρ (g cm^{-3})	1.0
Activation energy, E_o (J mol^{-1})	70,000
Reference temperature, T_{ref} (°C, K)	185 (458)
Specific heat, $C_{P,o}$ (erg g^{-1} K^{-1})	2.00×10^7
Relaxation time, λ (s)	0.3
Zero-shear-rate viscosity, η_o (Pa s)	90,000
Ideal gas constant, R (J mol^{-1} K^{-1})	8.314
Emissivity, ε	0.5
Stefan-Boltzmann constant (erg s^{-1} cm^{-2} K^4)	5.67×10^{-5}
Empirical constants, k_1 and k_2 (K^{-1}) in eq. (32)	1.454 and 0.000271
Coefficient of expansion, c_ρ in eq. (33)	0.00069
Heat transfer coefficient, H (erg cm^{-2} K^{-1})	6000.0
Bubble radius at die, r_i (cm)	1.0
Melt velocity at die exit, u_o (cm s^{-1})	1.0
Film thickness at die, h_o (cm)	0.1
Dimensionless length, L/r_o	5.0
Inlet temperature, T_o (°C, K)	185 (458)
Dimensionless force, f	2.9
Dimensionless pressure, B	0.2
Air temperature, T_{air} (°C, K)	25 (298)

Nonisothermal Maxwell case

To perform the nonisothermal simulations of reported experiments, a method for deriving the nonisothermal constitutive equation from the isothermal one must be chosen. The method of choice, reported by previous studies[28,30] when using integral constitutive equations, is the Morland–Lee hypothesis,[21] which applies time-temperature shifting by incorporating a

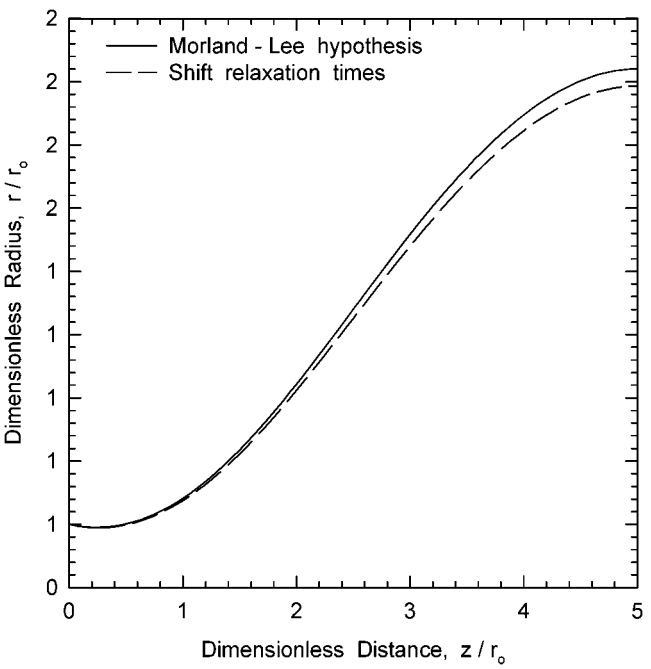

Figure 10 Predictions of the radius variable for the nonisothermal UCM viscoelastic simulations using the Morland–Lee hypothesis[21] and shifting the relaxation times with an appropriate shift factor.[22] Simulation conditions are given in Table IV.

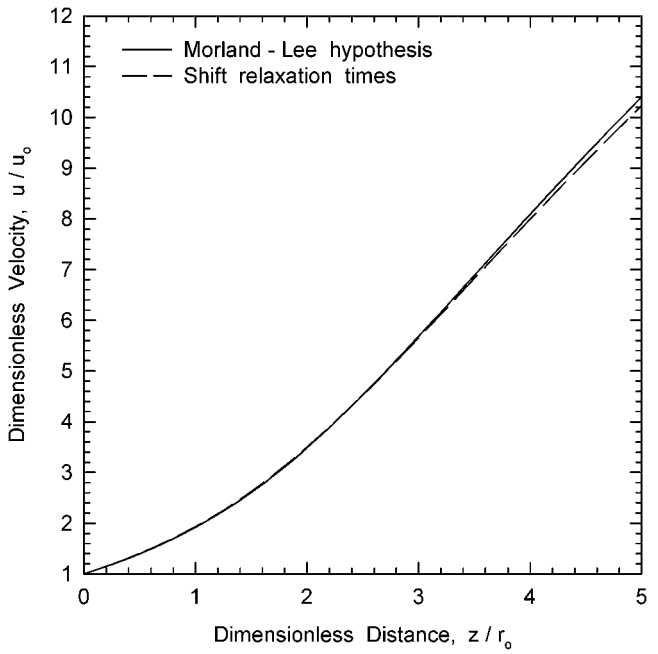

Figure 11 Predictions of the velocity variable for the nonisothermal UCM viscoelastic simulations using the Morland–Lee hypothesis[21] and shifting the relaxation times with an appropriate shift factor.[22] Simulation conditions are given in Table IV.

pseudotime measured by the material's own internal clock. However, the opportunity is offered here to compare the Morland–Lee hypothesis[21] with the method of shifting the relaxation times [eq. (28)] as methods to evaluate nonisothermal stresses. Only the upper-convected Maxwell (UCM) model will be considered in this comparison. The operating conditions for this test case are given in Table IV. Figure 10 shows the radial profiles for both methods. There is no major difference in the radial profiles for both methods, except that the method of shifting the relaxation times produces a final dimensionless radius (r_L/r_o) somewhat lower than the Morland–Lee hypothesis. Figure 11 shows the velocity profiles for both methods, and again no major difference is observed. Finally, Figure 12 shows the temperature profile for both methods, and displays no major differences. Therefore, the method of shifting the relaxation times used by Luo and Tanner[22] does not differ significantly in results compared with applying the Morland–Lee hypothesis.[21] Both methods are capable of handling nonisothermal conditions when using integral constitutive equations. However, the Morland–Lee hypothesis has been chosen in this study because of its ease of implementation in the current numerical scheme, its speed and accuracy. This happens because it allows the use of the Gauss–Laguerre quadrature, which is well-suited for exponentially fading functions and requires only 15 positions in the particle's deformation history for the computation of the stresses given by the integral constitutive equation.

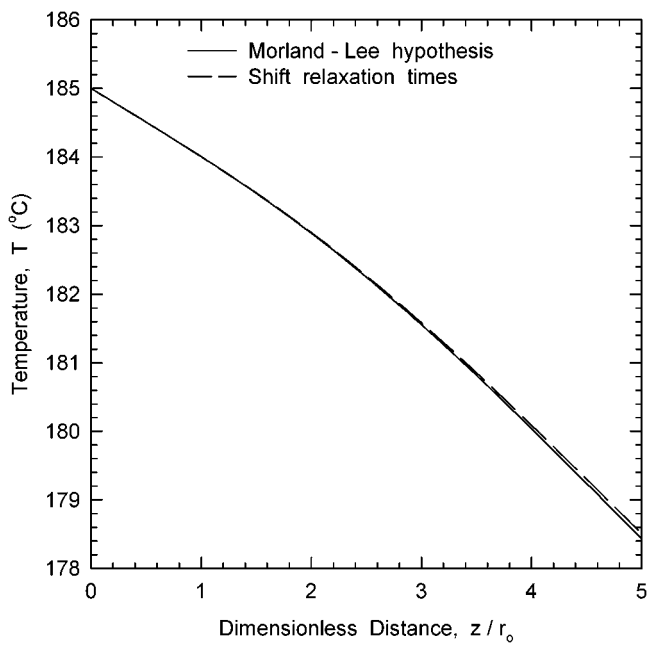

Figure 12 Predictions of the temperature variable for the nonisothermal UCM viscoelastic simulations using the Morland–Lee hypothesis[21] and shifting the relaxation times with an appropriate shift factor.[22] Simulation conditions are given in Table IV.

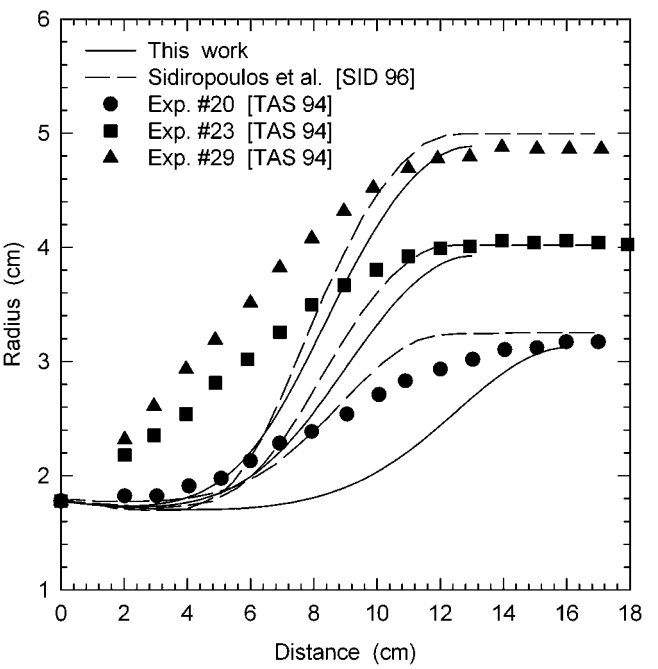

Figure 13 Comparison of current simulations with those of Sidiropoulos et al.[11] and experiments conducted by Tas[19] with the L8 Stamylan low-density polyethylene (LDPE) for the radius variable. Operating conditions are given in Table V with nonisothermal conditions given in Table II.

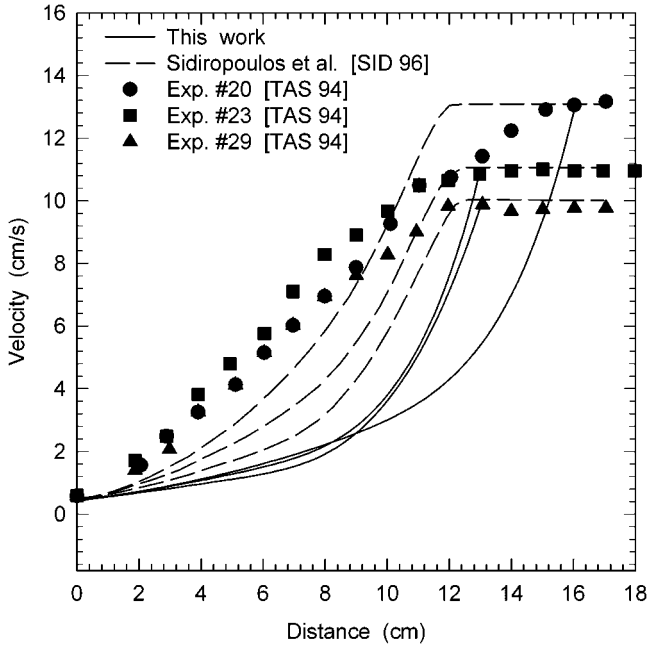

Figure 14 Comparison of current simulations with those of Sidiropoulos et al.[11] and experiments conducted by Tas[19] with the L8 Stamylan low-density polyethylene (LDPE) for the velocity variable. Operating conditions are given in Table V with nonisothermal conditions given in Table II.

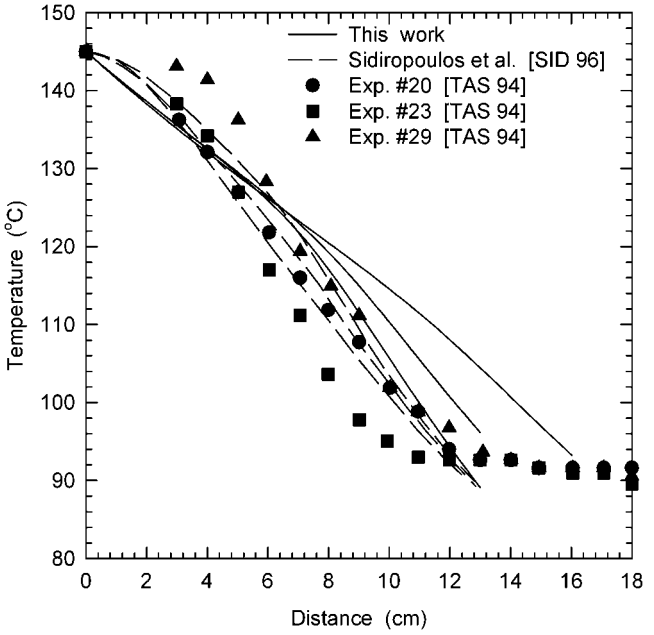

Figure 15 Comparison of current simulations with those of Sidiropoulos et al.[11] and experiments conducted by Tas[19] with the L8 Stamylan low-density polyethylene (LDPE) for the temperature variable. Operating conditions are given in Table V with nonisothermal conditions given in Table II.

Nonisothermal PSM case—Comparison with experiments

Experiments by Tas[19]

The comparison of numerical simulations to experiments performed by Tas[19] for the L8 Stamylan LDPE is presented in Figures 13–15 for the radius, velocity, and temperature, respectively. The operating conditions used for the simulations are taken from the reported experiments and given in Table V. The rheological characterization used for the simulations is given in Table I.

It can be seen from Figure 13 for Tas's[19] experiments nos. 20, 23, and 29 that the simulations have difficulty in predicting the correct bubble shape. The reason may be due to external forces not taken into account in the film-blowing governing equations. Such forces are aerodynamic forces coming from the turbulent jet of air used in cooling the bubble surface, air drag, gravity, and inertia. Surface tension can be assumed to be negligible in most polymer melt operations, and so are gravity and inertia.[2] Also included in the figures are the predictions from Sidiropoulos et al.,[11] who used a nonisothermal purely viscous model. Figure 13 shows that the results from Sidiropoulos et al.[11] and the current results do not differ much except for experiment no. 20. The reason for this difference in experiment no. 20 is the choice of the position of the freezeline. Sidiropoulos et al.[11] chose a freezeline closer to the die than the current simulation. Another reason for the discrepancy between simulation and experiments is the problem of multiple solutions, which results when using the current film-blowing model. Other researchers[5,7,8,31,32] have also encountered difficulties in using the current thin-shell model, including multiplicities and instabilities.

The current method used to predict the bubble shape is to manually change the dimensionless pressure, B and the dimensionless force, f, until the final radius, r_L, and the final velocity, u_L, in the simulations matches that of the experiments. Shown in Table VI are the results from the simulations for the dimensionless force and pressure compared with the experiments. The simulations under-predict the experi-

TABLE V
Film-Blowing Operating Conditions for Simulation Based on Experiments with L8 Stamylan LDPE Conducted by Tas[19]

Property (units)	Value
Bubble radius at die, r_i (cm)	1.78
Melt velocity at die exit, u_o (cm s^{-1})	0.4198
Film thickness at die, h_o (cm)	0.22
Dimensionless length, L/r_o	10.0
Inlet temperature, T_o (°C, K)	145 (418)
Air temperature, T_{air} (°C, K)	25 (298

TABLE VI
Comparison Between Experimental and Predicted Inflation Pressures and Tension Forces for the Experiments with L8 Stamylan LDPE Conducted by Tas[19] and Simulations Conducted by Sidiropoulos et al.[11]

Run no.	Measured force (*N*) [Ref. 19]	Predicted force (*N*)		Measured pressure (Pa) [Ref. 19]	Predicted pressure (Pa)	
		This work	Ref. 11		This work	Ref. 11
20	3.80	1.60	1.05	78	198	170
23	4.30	1.86	1.20	85	186	150
29	3.50	2.13	1.30	70	168	120

ments for the force and over-predict the experiments for the pressure for all three cases. However, the viscoelastic simulations predict forces closer to the experiments than that of Sidiropoulos et al.[11] with the nonisothermal purely viscous simulations. Once more, this may be due to the inability of the model to capture all of the forces exerted on the blown film. The model is closer in predicting the force and pressure at higher BUR conditions. Figure 14 displays the comparison between simulations and experiments for the velocity variable. Also included in Figure 14 are the simulations of Sidiropoulos et al.[11] Again, there is a large discrepancy for the velocity profile of the current simulations and those of Sidiropoulos et al.[11] for experiment no. 20. As stated earlier, this is due to the choice of position of the freezeline.

Figure 15 shows the simulated and experimental temperature profiles for all three cases. The simulated temperature profiles agree well with the experimental temperature profiles for all three cases. However, from Table II, the heat transfer coefficient required in the simulations to obtain the proper temperature profile is 10 times that used in other reported simulations.[7,8] It is possible that Tas[19] used higher velocities of cooling air to solidify the bubble. The principal reason for the discrepancy is the inability of the model, specifically eq. (29), to take into effect the convection caused by turbulent air surrounding the bubble. A better relation is required to relate the heat transfer coefficient, *H*, in eq. (30), which takes into account the velocity of air surrounding the bubble. Such relations exist for cross-flow air with cylinders and plates but do not exist for complicated situations such as this one (cocurrent turbulent air with changing bubble radius).

In an attempt to discover why the simulations of Sidiropoulos et al.[11] gave slightly better values for the film radius (*r*) and the film velocity (*u*), the uniaxial viscosity (η_E) and the biaxial viscosity (η_B) were calculated as a function of distance from the die. Figure 16 shows both viscosities for the K-BKZ integral constitutive model, eq. (16), for the L8 Stamylan LDPE, as well as the Newtonian model with the same zero-shear-rate viscosity. Also shown in Figure 16 is the magnitude of the extensional-rate tensor, defined as:

$$\left|\bar{\bar{\dot{\varepsilon}}}\right| = \sqrt{\frac{1}{2} II_{\dot{\varepsilon}}} = \left[\frac{1}{2}\bar{\bar{\dot{\varepsilon}}} : \bar{\bar{\dot{\varepsilon}}}\right] \tag{47}$$

where the extensional-rate tensor is given by:

$$\bar{\bar{\dot{\varepsilon}}} = 2\ \cos\theta \begin{bmatrix} \frac{du}{dz} & 0 & 0 \\ 0 & \frac{u}{r}\frac{dr}{dz} & 0 \\ 0 & 0 & -\frac{du}{dz} - \frac{u}{r}\frac{dr}{dz} \end{bmatrix} \tag{48}$$

Eqs. (47) and (48) were used to find the extensional rates along the film needed for the K-BKZ model, eq. (16). The temperature dependence of the viscosities from the K-BKZ model and the Newtonian model was formulated as

$$\eta(T) = \eta(T_{\text{ref}})a_T \tag{49}$$

where the shift factor a_T is defined as in eq. (27). Figure 16 shows that the Newtonian model gives higher

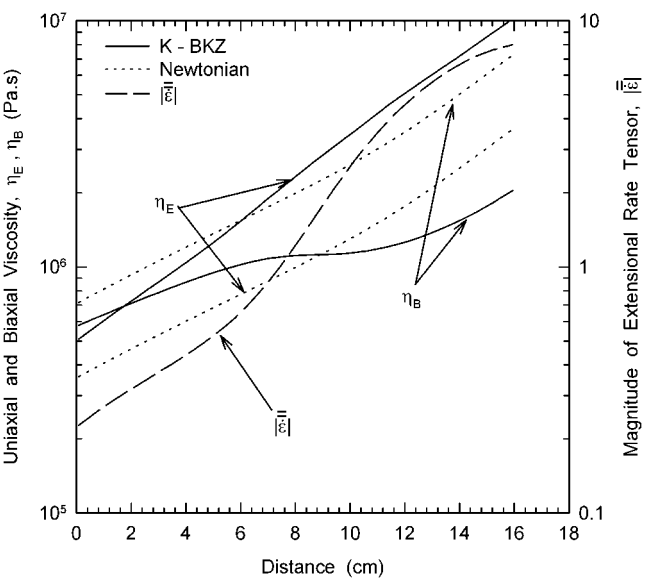

Figure 16 Uniaxial viscosity (η_E) and biaxial viscosity (η_B) as a function of distance from the die for the L8 Stamylan low-density polyethylene (LDPE), using the K-BKZ model, eq. (16), and the Newtonian model. The material parameters used for the K-BKZ model are given in Table I. The Newtonian viscosity was derived from the zero-shear-rate viscosity of the L8 Stamylan LDPE.

predictions for the biaxial viscosity (encountered during the film-blowing process) than that of the K-BKZ model. This might explain why the predictions for the radius and velocity were slightly better. It may also explain why the velocity variable for the simulations of Sidiropoulos et al.[11] shows a plateau near the freezeline (the current numerical scheme in terms of the velocity variable does not show a plateau), which parallels the film-blowing process in reality.

Experiments by Gupta[18]

Previous simulation attempts[7,8,10] have used for comparison the experimental data by Gupta,[18] and in particular experiment no. 20 for the Styron 666 PS. The first two simulation attempts have used the nonisothermal UCM model with a single relaxation time and a temperature-dependent viscosity, and showed that agreement could be obtained with the experiments only by choosing appropriately some constants, that do not necessarily reflect the proper experimental conditions. The attempt by Alaie and Papanastasiou[10] with the current PSM model showed a surprisingly good agreement with the experiments.

In our efforts to simulate Gupta's results we also used the same rheological characterization as done by Alaie and Papanastasiou.[10] It should be noted that the final Weissenberg number for this simulation ($Ws = 1.82$) indicates a highly viscoelastic flow. Consequently, this high viscoelastic flow was unattainable in this study, and results were only obtained up to a Weissenberg number of $Ws = 0.90$ (i.e., the die velocity, u_o, in eq. (18) was not reached in simulations while increasing the viscoelasticity of the material). This results in the material not being as viscoelastic in the simulations as it is in the experiments.

Alaie and Papanastasiou[10] used a shear prehistory, which gives oscillatory stresses at high Weissenberg numbers, as shown earlier in Figure 8. Also they have not shown any results for high Weissenberg numbers in their previous simulations, and even the limiting case for $Ws = 0.001$ shows discrepancies from the Newtonian solution. These facts raise serious questions about the validity of the study conducted by Alaie and Papanastasiou.[10] Another work[12] has also raised questions concerning the study by Alaie and Papanastasiou[10] with regard to the simulation of Gupta's experiments.[18] In particular, it refers to the ratio of the machine stress to the hoop stress, τ_{ss}^*/τ_{tt}^*. Kurtz[12] stated that there must have been an error in converting units, which was initially done by Gupta.[18] However, it is unlikely that Alaie and Papanastasiou[10] repeated this error since with the operating conditions as boundary conditions, the simulations should have uncovered this error automatically and should not have been repeated. Kurtz[12] also states that for the given film-blowing governing equations [eqs. (8) and (9)], the machine direction stress, τ_{ss}^*, should always be greater than the hoop stress, τ_{tt}^*. In their corresponding figure, Alaie and Papanastasiou[10] report the hoop stress to be larger than the machine-direction stress, which is impossible with the current film-blowing governing equations. Our own simulations always gave results for the stress ratio in agreement with Kurtz's statement. It appears, therefore, at present that the experimental data by Gupta have not been successfully simulated in the open literature with a fully nonisothermal viscoelastic model.

CONCLUSIONS

Numerical viscoelastic simulations have been undertaken for the film-blowing process. The governing equations used are those introduced earlier by Pearson and Petrie.[1,2] Isothermal Newtonian and upper-convected Maxwell (UCM) results have been successfully reproduced using an integral constitutive equation of the K-BKZ type. Shear prehistory in the evaluation of the integral stresses was compared with extensional prehistory, and the latter was proven to be superior, resulting in smooth stress profiles. Nonisothermal viscoelasticity has been handled both by the Morland–Lee hypothesis, using a pseudotime time-temperature shifting method, and by an alternative method, which shifts the relaxation times by the appropriate shift factor. The two cases have been examined for the Maxwell model case and were shown to give almost identical results. The Morland–Lee hypothesis is preferred due to its efficiency.

Comparison of numerical simulations with experiments on a polymer melt (LDPE) resulted in poor qualitative agreement in terms of bubble radius and film velocity. Also, the numerical predictions underestimate the force and overestimate the pressure. The reason for this disagreement was attributed to the inability of the governing model (thin-shell approximation and force balances) to take into effect mainly the aerodynamic forces from the turbulent air mass cooling the film from outside the bubble. However, the current simulations showed good agreement with previous nonisothermal simulations[11] employing a purely viscous model. Therefore, a nonisothermal viscoelastic model does not give better predictions than a nonisothermal Newtonian model, contrary to previous suppositions.[11] Comparisons were also made with a previous simulation conducted by Alaie and Papanastasiou,[10] which raised serious questions concerning their study.

The stability of the film-blowing numerical scheme has been previously studied[7] for Newtonian and Maxwell fluids, where multiplicities are to be expected.

However, the discrepancy between the current simulations and experiments is more than likely not because of multiplicities, but rather an inability of the model to accurately predict the forces exerted on the film. Emphasis is again given to the effects of aerodynamic forces from turbulent cooling air supplied to the bubble.

References

1. Pearson, J. R. A.; Petrie, C. J. S. J Fluid Mech 1970, 40, 1.
2. Pearson, J. R. A.; Petrie, C. J. S. J Fluid Mech 1970, 42, 609.
3. Han, C. D.; Park, J. Y. J Appl Polym Sci 1975, 19, 3257.
4. Kanai, T.; White, J. L. Polym Eng Sci 1984, 24, 1185.
5. Petrie, C. J. S. Rheol Acta 1973, 12, 92.
6. Wagner, M. H. Rheol Acta 1978, 15, 40.
7. Cain, J. J.; Denn, M. M. Polym Eng Sci 1988, 28, 1527.
8. Luo, X.-L.; Tanner, R. I. Polym Eng Sci 1985, 25, 620.
9. Cao, B.; Campbell, G. A. AIChE J 1990, 36, 420.
10. Alaie, S. M.; Papanastasiou, T. C. Int Polym Proc 1993, 8, 51.
11. Sidiropoulos, V.; Tain, J. J.; Vlachopoulos, J. J Plast Film Sheeting 1996, 12, 107.
12. Kurtz, S. J. Int Polym Proc 1995, 10, 148.
13. Minoshima, W.; White, J. L. J NonNewtonian Fluid Mech 1986, 19, 275.
14. Ghaneh-Fard, A.; Carreau, P. J.; Lafleur, P. G. J Plast Film Sheeting 1996, 12, 68.
15. Ghaneh-Fard, A.; Carreau, P. J.; Lafleur, P. G. AIChE J 1996, 42, 1388.
16. Ghaneh-Fard, A.; Carreau, P. J.; Lafleur, P. G. Int Polym Proc 1997, 12, 136.
17. Ghaneh-Fard, A.; Carreau, P. J.; Lafleur, P. G. Polym Eng Sci 1997, 37, 1148.
18. Gupta, R. K. A New Non-Isothermal Rheological Constitutive Equation and its Applications to Industrial Film Blowing Processes, Ph.D. Thesis, Department of Chemical Engineering, University of Delaware, Newark, DE, 1980.
19. Tas, P. P. Film Blowing: From Polymer to Product, Ph.D. Thesis, Department of Mechanical Engineering, Eindhoven University of Technology, Eindhoven, The Netherlands, 1994.
20. Papanastasiou, A. C.; Scriven, L. E.; Macosko, C. W. J Rheol 1983, 27, 387.
21. Tanner, R. I. Engineering Rheology; Clarendon Press: Oxford, 1985.
22. Luo, X.-L.; Tanner, R. I. Rheol Acta 1987, 26, 499.
23. Luo, X.-L.; Tanner, R. I. Int J Num Methods Eng 1988, 25, 9.
24. Haw, J. A Study of Tubular Film Blowing Process, Ph.D. Thesis, Department of Chemical Engineering, Polytechnique Institute, New York, 1984.
25. Peters, F.; Ruppel, C. Int Polym Proc 2006, 21, 319.
26. Zhang, Z.; Lafleur, P. G.; Bertrand, F. Int Polym Proc 2006, 21, 527.
27. Chen, Z.; Papanastasiou, A. C. Int Polym Proc 1987, 2, 33.
28. Barakos, G.; Mitsoulis, E. J NonNewtonian Fluid Mech 1996, 62, 55.
29. Beaulne, M. Viscoelastic Characterization of Complex Materials and Modeling of Forming Processes, M.Sc. Thesis, Department of Chemical Engineering, University of Ottawa, Ottawa, ON, Canada, 1998.
30. Rauschenberger, V.; Laun, H. M. J Rheol 1997, 41, 719.
31. Han, S.; Becker, E. Rheol Acta 1983, 22, 521.
32. Han, S. Chem Eng Commun 1985, 33, 307.